

# Rapid Near-Infrared Qualification of Microcrystalline Cellulose and Sodium Caprate Minitablets Through Intact Enteric Coated Capsules

<sup>1</sup>Joseph Medendorp, <sup>1</sup>Joseph Wyse, <sup>1</sup>Robert A. Lodder, <sup>2</sup>Lloyd G. Tillman, <sup>2</sup>Sujatha Sonti and <sup>1</sup>Michael Jay

<sup>1</sup>Department of Pharmaceutical Sciences and Center for Pharmaceutical Science & Technology, University of Kentucky

<sup>2</sup>Isis Pharmaceuticals

## Introduction

In this study we show the application of a nondestructive process analytical technology to separate two populations of enteric coated capsules that contained minitables. In the course of a small, phase I clinical trial investigation it was deemed necessary to have two different placebo capsule formulations that were matched in appearance. These capsule batches were manually filled wherein subsequent processing required that they be specifically identified and accordingly classified (i.e., sorted). The sorting was based on a near-infrared (NIR) spectral differentiation between the capsule fill of the two formulations. Both capsule lots appear identical as enteric coated: white (titanium dioxide) hard gelatin capsules having an orange band. One lot contains pure microcrystalline cellulose (MCC) minitables while the other lot contains minitables composed principally of sodium caprate (C10) with PEG 3350 added as a binder. The enteric coating used on both lots is composed of methacrylate polymers with plasticizers at a cured coating level of approximately 14 mg solids per cm<sup>2</sup> of capsule surface area. In order to facilitate a streamlined manufacturing schedule, it was necessary to rapidly develop and GMP qualify a technically feasible, nondestructive capsule identification and sorting process.

Near-infrared (NIR) spectroscopy has successfully been applied to the noninvasive and nondestructive differentiation of various capsules, tablets, and drugs in solution [1-5]. While current scholarship

suggests that NIR is fairly well established for this purpose, previous studies focus on the utility of NIR for the quantification and identification of capsules filled with powders and solutions. In the current case, the formulations in the capsules (methacrylate coated, orange-banded, hard gelatin) were not powders or solutions, but were minitables. Due to the large particle size (2 mm) and random orientation of the minitables in the capsules, the NIR absorbance spectra demonstrated more variation than a uniformly filled powder capsule. The combined effect of the enteric-coated hard gelatin exterior, and the random distribution of the minitab interior, made analysis of these capsules potentially more challenging than those in previous experiments. We undertook a combination of selective wavelength analysis along with chemometric principles to develop a non-destructive method for distinguishing between these two capsules. The method was subjected to validation testing using a calibration set and was ultimately used to sort through two populations of capsules totaling 3407 units using only two near-IR wavelengths provided by interference filters from a tungsten-halogen source. Such a simple instrument can be easily manufactured and widely deployed as a process sensor.

## *NIR Spectrometry and Chemometrics*

The near-infrared region of the electromagnetic (EM) spectrum covers wavelengths from 750 nm to 3000 nm. This region consists of

broad, overlapping peaks that result from overtone bands, combination bands, and difference bands from molecular vibration of CH, NH, OH, and SH bonds [6]. Many factors contribute to the variations in NIR spectra, such as detector noise, environmental conditions, and different sample preparation. Often the largest variations come from the constituent or concentration differences. Using this knowledge, chemometric techniques such as principal axis transformation can be used to interpret complex overlapping spectra by placing the original spectral variables into a new, smaller coordinate axis system [7]. Calculation of the principal components is accomplished by a singular value decomposition of matrix  $A$  according to  $A=USV$ , where  $A$  is the matrix of original spectra,  $U$  is the matrix of eigenvalues (scores),  $S$  is a diagonal matrix of singular values, and  $V$  is the matrix of eigenvectors (loadings). The first principal component may capture 80% or more of the total variance. Many of the eigenvalues model only noise, therefore only those that contain a significant proportion of the variation with analytical signal are used in calibration and evaluation of samples.

### BEST Algorithm

Principal components can be used to illustrate the separation of two groups. For a more quantitative result, the bootstrap error-adjusted single sample technique (BEST) was applied to the calibration data. The BEST algorithm begins by encoding the intensity on each wavelength as a separate dimension, thus reducing each spectrum to a single point in multidimensional space. Population  $P$  is an  $m \times n$  matrix in hyperspace  $R$  whose rows are the individual samples and the columns are the frequencies [8]. BEST considers each wavelength from a spectrum of  $n$  wavelengths to be taken as a separate dimension, such that each spectrum is reduced to a single point in  $n$ -dimensional hyperspace [3].  $P^*$  is a discrete realization of  $P$  based on a calibration set  $T$  of the same dimensions as  $P^*$ . This realization is chosen one time from  $P$  to approximate all possible sample variations present in  $P$ .  $P^*$  has parameters  $B$  and  $C$ , where  $C = E(P)$  and  $B$  is the Monte Carlo approximation to the bootstrap distribution. The expectation value,  $E(P)$ , is the center of  $P$ , and  $C$  is a row vector with the same number of rows as there are columns in vector  $P$ . New test spectra  $X$  are projected into hyperspace  $R$  containing  $B$ , rows of  $B$  are mapped onto a vector connecting  $C$  and  $X$ .  $C$  and  $X$  have the same dimensions. The integral over  $R$  is calculated from the center of  $P$  in all directions. A skew-adjusted standard deviation (SD) is based on the comparison of the expectation value  $C=E(P)$  and  $C=med(T)$ , the median of  $T$  in hyperspace projected on the hyperline connecting  $C$  and  $X$ . The result is an asymmetric SD that provides two measures of the SD along the hyperline connecting  $C$  and  $X$ . Equation 1 defines the SD in the direction of  $X$ , and Equation 2 defines the SD in the opposite direction. Skew adjusted SDs can be used to calculate mean distances between spectra of different samples.

$$+\sigma \frac{\int_0^{\infty} \int_0^{\infty} P^* \rightarrow (\overline{CX})}{\int_0^{\infty} P^* \rightarrow (\overline{CX})} = 0.34 \quad \text{Equation 1}$$

$$-\sigma \frac{\int_0^{\infty} \int_0^{\infty} P^* \rightarrow (\overline{CX})}{\int_0^{\infty} P^* \rightarrow (\overline{CX})} = 0.34 \quad \text{Equation 2}$$

## Methods

### Separation of MCC and C10 Capsules with Full NIR Spectra

The first objective was to prove that full NIR spectra from 1100-

2500 nm (in 2 nm steps with 10 nm bandpass) could be used to separate the MCC and C10 capsules. Initial experiments involved only three MCC capsules and three C10 capsules. Spectra were collected with a scanning monochromator instrument. Each capsule was scanned three times for a total of 18 spectra (Figure 1).

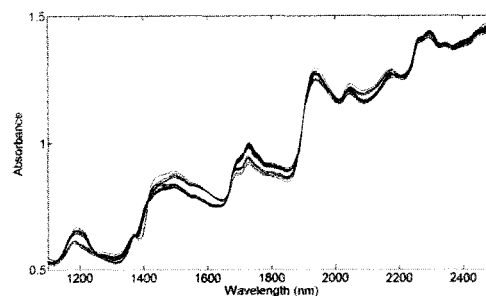


**Figure 1. Broadband NIR spectra of C10 (blue) and MCC (red) capsules collected with a scanning monochromator instrument.**

The capsules were scanned in random order and rotated following each scan to average possible sample variations due to inconsistencies in the enteric coating, gelatin layer and the orientation of the minitables. Scans were collected inside of an instrument drawer to eliminate room noise and external interferences. Data were multiplicative scatter-corrected to eliminate baseline variations [9], and second derivatives [10] were plotted to find the regions in the spectrum where the most variation was apparent (Figure 2).

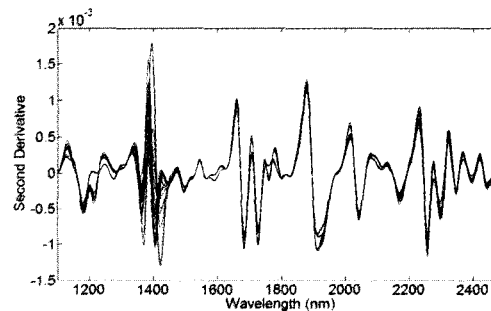


**Figure 2. Second derivative spectra calculated from the broadband spectra of C10 (blue) and MCC (red) capsules.**

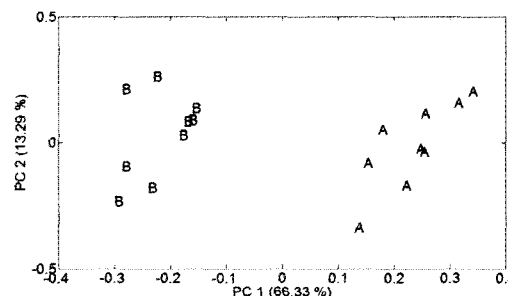


**Figure 3. The two-dimensional principal component plot from broadband calibration data demonstrates how closely the capsules cluster in space, C10 capsules (marked with 'A') project on the right and MCC capsules (marked with 'B') project on the left.**

Principal components (PCs) were calculated and the PCs with the largest contribution to variation were plotted in two and three

dimensions to visualize the differences between capsule groups (Figures 3 and 4) [7]. BEST standard deviations and cross-validation standard deviations (CV-SD) provided a quantitative measure of group separability [3,8].

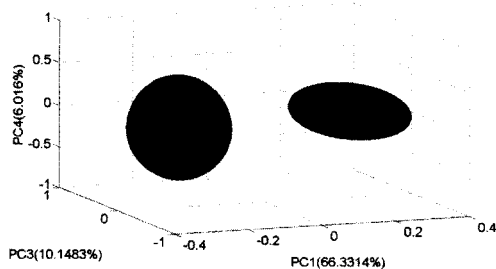


**Figure 4. Three-dimensional principal component (PC) plot from broadband NIR spectra. The majority of the separation is seen along the PC 1 axis, which captures 66.33% of the total variation. This separation suggests that the difference in capsule constituents, C10 (blue) vs. MCC (red), is mainly responsible for the separation between the two groups of spectra.**

In order to estimate the limits of detection for the NIR, a cluster translation procedure was performed [11]. NIR spectra from the two capsule populations,  $P_1$  and  $P_2$  are expressed in  $m \times n$  matrices, where  $n$  is the number of wavelengths and  $m$  is the number of spectra. The columns of the matrices are averaged by Equations 3 and 4, giving two  $1 \times n$  vectors.

A difference spectrum  $X$  is calculated from  $P_{2ave} - P_{1ave}$ . One population was spatially translated toward the other,  $P_{Adjusted} = y * X + P_2$ , where  $y$  starts at zero, increasing in increments of 0.01 until  $P_1$  and  $P_{Adjusted}$  are inseparable. It is assumed that the two capsule groups represent the possible variations in the pure component spectra (MCC and C10), and that all points on the hyperline connecting the centers of the two population distributions correspond to mixtures of the two components because the Beer-Lambert Law holds. For example, when one population is translated one-half the distance toward the other, that population corresponds to a 50/50 mixture of MCC and C10. The maximum distance the two groups can move toward each other while maintaining statistical separation determines the minimum quantities of MCC and C10 that can be detected in each other.

$$P_{1ave} = \frac{1}{m} \sum_{i=1}^{i=m} P_{1i} \quad \text{Equation 3}$$

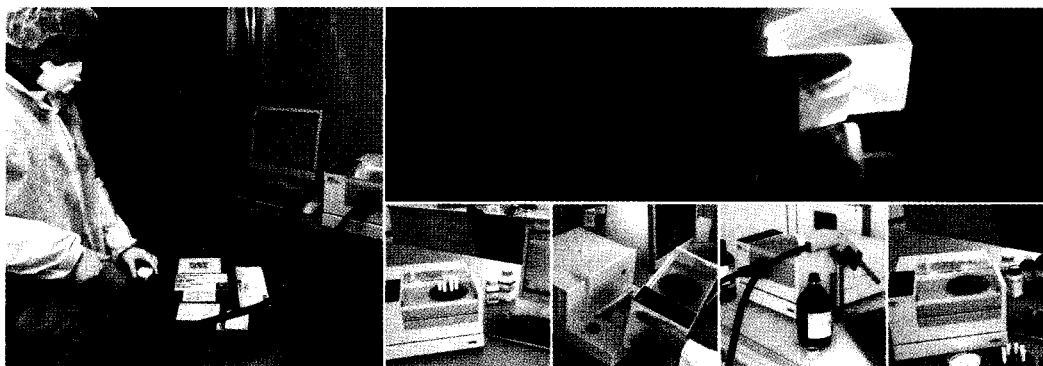
$$P_{2ave} = \frac{1}{m} \sum_{i=1}^{i=m} P_{2i} \quad \text{Equation 4}$$

### *Rapid Separation of MCC and C10 Capsules with Fewer Wavelengths*

Although the overall goal of this project was to develop a process analytical method sensitive enough to assign the MCC and C10 capsules to their respective groups accurately, it was also imperative that

## From Material ID to PAT Qualitative & Quantitative

**BUCHI**



**Precalibrated & Rugged. Ready to Use.**

Buchi can provide NIR Solutions for analytical needs from warehouse to process. Research grade performance in a rugged and flexible design. Buchi's unique FT NIR hardware, chemometrics software, calibration, validation and implementation services ensures the success of your NIR project. Visit our website to learn more and call us to discuss your applications or arrange for a presentation of the newest FT NIR System.

**Buchi, Inc.**

1.866.652.5238

[www.buchi-analytical.com](http://www.buchi-analytical.com)

Please circle #5

*Quality in your hands*

the project be completed as quickly as possible. This time constraint required a modification of the full spectrum approach. Experiments were conducted to accomplish the separation with as few wavelengths as possible, yet still with adequate statistical assurance of specificity. Using the same six capsules scanned above at 701 wavelengths, new spectra were collected with a 19-wavelength filter wheel NIR spectrometer between 1445 and 2348 nm.

Capsules were placed in the conical reflective cup oriented with the thicker cap end down, body end up, and held in place with a steel rod (Figure 5). The conical reflecting cup is designed such that when a sample capsule is placed along the axis of radial symmetry of the cone, specular reflection at the detector is minimized while diffuse reflectance is maximized [2].

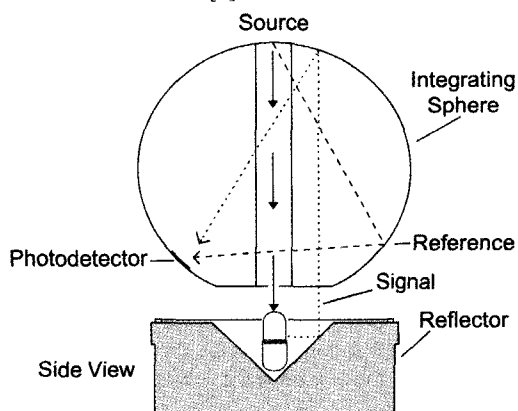


**Figure 5. 90° conical reflective cup used as a capsule holder. The cup is designed so that when a sample capsule is placed along the axis of radial symmetry of the cone, specular reflection at the integrating sphere detector is minimized while diffuse reflectance is maximized. As a result, the majority of the light reaching the detector has been scattered by the contents of the capsules.**

All radiation that follows a path parallel to the incident beam and perpendicular to the base of the conical reflector is reflected and collimated back toward the source. This radiation is predominantly specular reflectance and contains little information about the capsule fill. In the same fashion, a small amount of radiation that passes through the capsule but does not scatter is also returned to the source. Therefore, the majority of the radiation reaching the detector via the integrating sphere is scattered by the contents of the capsule. The amount of radiation that reaches any given location on the capsule is directly proportional to the curved surface area of the frustum (the conic section defined by two parallel lines from the light source, and a plane parallel to the reflector base connecting the two lines) in which it lies. Therefore, more light reaches the top of the capsule than the bottom of the capsule because there is more curved surface area at the top of the reflector than at the bottom.

The curved surface area is given by  $\pi s(r_1+r_2)$  where  $r_1$  and  $r_2$  are the radii of the base and top of a circular frustum,  $s$  is the length between the top and bottom measured along the surface of the cone. If the detector collected scattered light from cross-sections of the capsule, there would be a different intensity value for each cross-section. However, the detector uses an integrating sphere, which collects all of the scattered light from the entire capsule. This configuration eliminates the concern of uneven illumination along the capsule.

In order to best accommodate the capsules, the spectrometer was inverted, and an instrument drawer was fashioned for consistent and

reproducible sample loading. Each scan took approximately two minutes to collect the full 19 wavelengths. Capsules were scanned in random order and rotated to average sample positioning variations. Principal components, intercapsule BEST standard deviations (SDs), and intracapsule cross-validation standard deviations were calculated from the resulting spectra. Spectra for the two groups of capsules were very different, allowing a visual inspection of the spectra to sufficiently identify the more distinguishing wavelengths. Standard deviations and cross-validation-SDs were calculated from four selected wavelengths. To operate as quickly as possible while maintaining the highest level of capsule classification accuracy, the two most distinguishing wavelengths were selected by visual inspection. From these wavelengths, ratios were calculated and plotted to prove that the two wavelength approach was sufficient to justify exploration of a larger validation set.

### Equipment Calibration

The filter wheel spectrometer was installed in the GMP facility in the University of Kentucky Center for Pharmaceutical Science & Technology, and turned on for the remainder of the procedure to eliminate detector drift due to thermal variations. A polystyrene calibration film standard fitted to a conical reflective cup was scanned 50 times to capture all possible sample variations. A ratio was calculated from the signal intensity at 1734 nm and 1445 nm for each scan of polystyrene standards, and confidence limits were constructed around the mean at  $\pm$  six standard deviations,  $1.0245 \pm 0.0118$ . The choice of a 12 standard deviation acceptance range was made to ensure essentially 100% confidence limits on classifications for the set of 3407 capsules to be scanned. To prove that the instrument response was the same from day to day, these ratios were projected on top of the predefined constructed confidence limits.

The same approach was used to identify the different capsules. A calibration set consisting of 50 MCC and 50 C10 capsules was scanned. Wavelength ratios were calculated and confidence limits were constructed at the mean  $\pm$  six standard deviations for each of the two capsule formulations. These limits were defined as the acceptance criteria boundaries for the determination of which group the incoming capsule belonged (Figure 6).

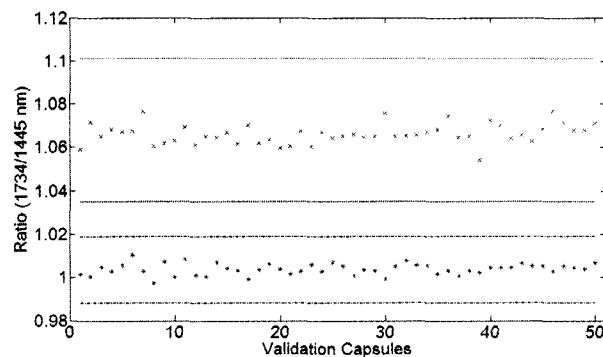


**Figure 6. Ratio of the signals at 1734 and 1445 nm from the validation set of capsules. The steeper curve has the higher ratio, thus C10 projects on top (x), and the flatter curve has a lower ratio so the MCC capsules project on the bottom (\*). The bars above and below the data sets are the confidence intervals, placed at six standard deviations above and below the mean.**

## Capsule Identification Screening Using the Reduced-Wavelength Approach and Confidence Limits

At the start of each day of data collection, the polystyrene calibration standard was scanned to prove the instrument was performing reproducibly. Capsules were sequentially scanned in groups of 20; a total of 3407 capsules were scanned. An algorithm was written to automatically calculate and display the wavelength ratios on top of the predefined confidence intervals (Figure 7). Capsules were sorted according to where their NIR ratios projected relative to the calibration experiments.

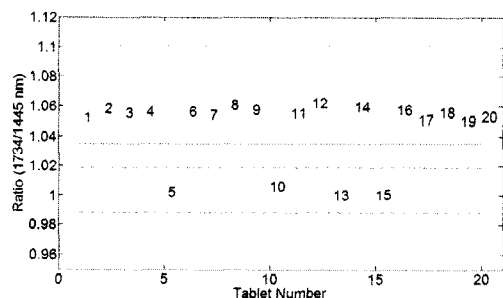


**Figure 7. Real data sets were collected in groups of twenty capsules. An algorithm was written to output this plot to show the two-wavelength ratio for each capsule.**

## Results and Discussion

Figure 8 illustrates the two wavelengths that were selected to distin-

guish between the two groups of capsules. The inert MCC has a relatively flat spectrum, while C10 has a very steep spectrum at these wavelengths. It is this spectral feature that allowed the simple calculation of a ratio from two wavelengths to distinguish between the two groups.

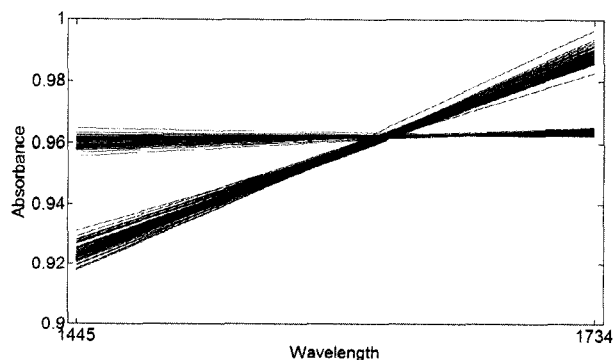


**Figure 8. Data collected with a filter wheel spectrometer at two NIR wavelengths (1734 nm and 1445 nm) collected from the two capsule validation set. MCC is the flat curve and C10 is the steeper curve. Of the 100 spectra displayed in this plot, there is obviously no overlap between the two different groups.**

Cross-validation results and the BEST standard deviations between capsules are reported in Table 1 for the full spectrum NIR measurements, for four wavelengths, and for two wavelengths. Note that the standard deviations are the same magnitude with two wavelengths as with the full

## Process Running

### Faster with CORONA Dryer and Blender from Carl Zeiss

Greater efficiency, higher productivity, and lower costs for pharmaceutical production processes can be realized by using Zeiss process NIR spectrometer systems.

By using the CORONA Dryer and Blender the following benefits can be obtained:

- Reduce the drying and blending time and minimize waste
- No time is lost due to sampling and waiting for lab results
- Non-invasive measurements at high speed using the latest diode array technology
- Produce quality product first time
- No operator contact

Contact us and find out more on how we can help to improve your process.

#### CORONA Dryer and Blender versions:

- IP 65 housing
- High-alloyed steel housing for GMP requirements (☉ II3D)
- EExP housing for use in hazardous areas
- Wireless communication with battery operation for blending



Carl Zeiss Microlmaging, Inc  
1 Zeiss Drive  
Thornwood, NY  
1059  
1-800-233-2343  
www.zeiss.com/micro



Please circle #6

spectra, suggesting that the basis of selectivity is improved by focusing on those wavelengths which can unequivocally distinguish between groups. This approach justifies and allows for a much smaller data set with which to base the classification upon. Illustrated in Figure 9 are the ratios (1734/1445 nm) calculated from all capsules projected into the confidence intervals determined during the calibration stage of the experiment.

This experiment resulted in greater than 99.71% successful capsule identification. Of the 3407 capsules scanned, ten capsules projected directly on or just outside their respective decision boundaries. These outliers were scanned a second time at the end of the experiment, and their two-wavelength ratios projected inside their respective confidence intervals.

Broadband	MCC	C10
MCC	1.70	29.54
C10		1.85
4 $\lambda$	MCC	C10
MCC	1.52	25.56
C10		1.58
2 $\lambda$	MCC	C10
MCC	1.24	23.46
C10		1.27

**Table 1. BEST standard deviations reported for the broadband, 4 wavelength, and 2 wavelength calibration data. Using the BEST, a successful measure of statistical separation between two populations was defined as a standard deviation greater than three, and a measure of statistical inseparability was a standard deviation less than three. The table reports intercapsule standard deviations, all greater than three, and reports intracapsule standard deviations along the diagonal, all less than three.**

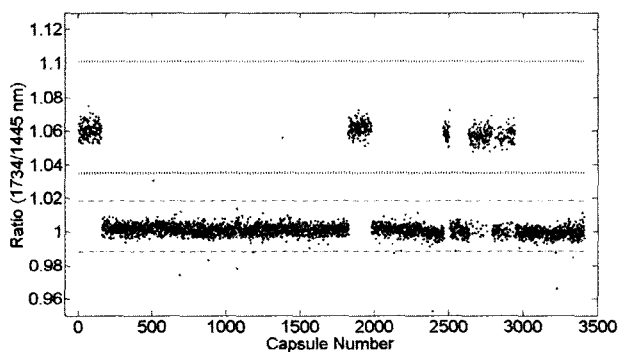


**Figure 9. Two-wavelength ratios from all 3407 capsules projecting inside their respective confidence intervals, C10 (top clusters) and MCC (bottom clusters). This figure illustrates greater than 99% successful identification.**

These results proved that the unclassified capsules were a result of erroneous manual sample loading, and further demonstrated the consistency and integrity of both the method of analysis as well as the capsules themselves.

Detection limits were estimated by the spatial cluster translation experiment described in the Methods above. When using MCC capsule spectra as the calibration set and C10 capsule spectra as the test set, C10 capsules could be spatially translated 92% of the distance across space before the populations were inseparable. When using C10 as the calibration set and MCC as the test set, MCC was spatially translated 89% of the distance across space before the populations were inseparable. This

demonstrates that NIR is capable of nondestructively identifying mixtures of C10/MCC in the capsules down to approximately ten percent of each one in the other. It is apparent that the NIR detection limits far exceed what is necessary to distinguish between MCC and C10 capsules.

## Conclusion

This study presents an effective application of NIR spectroscopy to the noninvasive and nondestructive classification of MCC and C10 minitables contained in enteric-coated (methacrylate polymer) hard gelatin capsules. The experiment was conducted in a GMP facility and is relevant to PAT. It was a very rapid method with data collection times of only 10 seconds, and the two wavelength approach gave unequivocal separation between the two capsules. The entire process, from conception to completion, required only 20 days. Of the 3407 capsules scanned, greater than 99.71% projected into their respective confidence intervals. Of the ten capsules that initially failed to validate, it was proven that human sample loading errors were responsible, suggesting that an automated version of the same experiment could have classified 100% of the capsules correctly. One of the primary goals of the FDA PAT initiative is to increase automation to reduce human error. This experiment provides an example of the benefits of automation, as well as of the utility of a method for real-time characterization and release of individual drug products.

New measurement, control and information technologies are needed in PAT to predict, control and assure product quality and performance. Using an appropriate PAT sensor, product quality attributes can be accurately and reliably predicted over the design space established for the materials used, the process parameters, and the environmental and other conditions. A two-wavelength near-IR sensor for PAT will be rugged, inexpensive, and simple to construct using two interference filters and a detector (e.g., PbS or InGaAs). Such a sensor would be a dynamic tool for process innovation and continuous quality improvement using risk-based models for inspection.

## Acknowledgements

The authors are grateful for the partial support from both the Kentucky Science and Education Foundation (KSEF-148-502-03-61) and the National Institutes of Health (N01AA 33003). The authors would also like to acknowledge the contributions of Jim Shanley and Jay Oliver of Isis Pharmaceuticals for their assistance in feasibility studies and Quality Assurance logistics.

## References

1. Lodder R, Hiefije G. *App. Spec.* 1988, 42, 556-558.
2. Lodder R, Selby M, Hiefije G. *Anal. Chem.* 1987, 59, 1921-1930.
3. Lodder R, Hiefije G. *App. Spec.* 1988, 42, 1500-1512.
4. Drennen JK, Lodder RA. *J. Pharm. Sci.* 1990, 79, 622-627.
5. Vergote GJ, Vervaeke C, Remon JP, Haemers T, Verpoort F. *Eur. J. Pharm. Sci.* 2002, 16(1,2), 63-67.
6. Burns D, Ciurczak E. *Handbook of Near-Infrared Analysis (Practical Spectroscopy) – 2nd edition.* Marcel Dekker; 2001.
7. Jolliffe IT. *Principal Component Analysis.* New York: Springer; 2002.
8. Hamilton S, Lodder R. *Proceedings of Society of Photo-Optical Instrumentation Engineers* 2002, 4626, 136-147.
9. Geladi P, MacDougall D, Martens H. *App. Spec.* 1985, 39, 491.
10. Maddams W, Southon M. *Spectrochim. Acta.* 1982, 38A, 459-466.
11. Drennen JK, Lodder RA. *Spectroscopy.* 1991, 6(8), 34-39.

Joseph Medendorp received his B.A. in Chemistry from Cornell University in 2002, and is currently a 4th year Ph.D. student in Pharmaceutical Sciences at the University of Kentucky. He is currently a UK-Center for Pharmaceutical Science and Technology Graduate Research Fellow.

Joseph Wyse, Ph.D., is the General Manager of the University of Kentucky Center for Pharmaceutical Science and Technology. Dr. Wyse has fourteen years of product and business development experience in the US pharmaceutical and biotech industry. His past positions include serving a group leader at Cryopharm Corporation (Pasadena, CA), manager at LifeCell Corporation (The Woodlands, TX) and associate director at Aronex Pharmaceuticals Inc. (The Woodlands, TX).

Robert A. Lodder, Ph.D. is currently Professor of Pharmaceutical Sciences at the College of Pharmacy, University of Kentucky Medical Center. Dr. Lodder holds joint appointments as a professor in the Departments of Chemistry and Electrical/Computer Engineering. He serves on the board of directors of Spherix and is a member of the U.S. Food and Drug Administration Advisory Committee on Pharmaceutical Science, Process Analytical Technologies subcommittee.

Lloyd Tillman, Ph.D., is Executive Director of Pharmaceutical Development at Isis Pharmaceuticals, Inc., Carlsbad, CA, where he is responsible for the formulation research, development and clinical manufacture of antisense oligonucleotide drug products. Prior to joining Isis, Dr. Tillman worked at the FDA from 1994 to 1997 as Associate Director over the Product Quality Research Laboratory.

Sujatha Sonti, Ph.D., is currently Associate Director, Technical Affairs at SkinMedica, Carlsbad, CA, where she is responsible for product development of topical formulations. Prior to joining SkinMedica, Dr. Sonti was responsible for formulation development and clinical manufacturing of oral and topical dosage forms at Isis Pharmaceuticals, Inc., Carlsbad, CA.

Michael Jay, Ph.D., is a Professor of Pharmaceutical Sciences in the College of Pharmacy at the University of Kentucky and the Director of the Center for Pharmaceutical Science & Technology. The Center has facilities for analytical method development and validation, stability studies, formulation development, and is home to an FDA registered pharmaceutical cGMP manufacturing facility.

To correspond with the authors, please contact the editor at: ay@russpub.com



Connecting People, Science and Regulation™



## 2006 PDA/FDA Joint Regulatory Conference



The Foundation for  
Business Success:  
Continuous Improvement  
Throughout the Product  
Life Cycle

SEPTEMBER 11-15

RENAISSANCE HOTEL  
WASHINGTON, D.C.

Conference  
September 11-13

Exhibition  
September 11-12

Training Courses  
September 14-15

Register  
early and  
save!

[www.pda.org/pdafd2006](http://www.pda.org/pdafd2006)

### What will it take to change the performance of the drug industry from acceptable to exceptional?

#### Find out at this year's PDA/FDA Joint Regulatory Conference!

Industry executives and academics will come together with FDA authorities in an unbiased, science-based forum, to discuss how the pharmaceutical industry can improve its performance by incorporating *Continuous Improvement Throughout the Product Life Cycle*. Hear directly from FDA representatives as they outline the Agency's expectations for current and emerging regulatory guidelines, as well as how industry is implementing these guidelines throughout the organization in such key areas as development, manufacturing, quality and regulatory science.

#### Take home strategies to build a better foundation for your organization's success:

- ▶ Integrate quality into your global business platform
- ▶ Leverage continuous improvement concepts across the value chain to link R&D, the supply chain, management and other functional groups
- ▶ Incorporate non-traditional solutions to build quality into the product life cycle

Please circle #7

# Process Analytical Technology and Multivariate Statistical Process Control

## Wellness Index of Product *and* Process – Part 3

Theodora Kourti, Ph.D.  
McMaster University

### Introduction

This series of papers discusses the important role that multivariate statistical projection methods have to play within the context of the FDA guidance on Process Analytical Technology (PAT). In the last 15 years several industries (food, petrochemical, polymer, semiconductor, steel) adopted these methods and managed to achieve (and exceed) the goals described by PAT [1-3]. These methods are superb tools for handling and analyzing large databases of noisy, correlated data with missing measurements, which are typical in industry. They have been successfully utilized for process analysis, understanding, and troubleshooting. They have also found their way to multivariate statistical process control (MSPC) and fault detection and isolation. With MSPC one can monitor the wellness of the process and product, by looking simultaneously at hundreds of variables collected in real time. By doing this, not only acceptable end product quality at the completion of the process as defined by the FDA is ensured, but at the same time continuous monitoring of the “overall process signature” or the “wellness of the process” itself occurs. MSPC will detect events such as thermocouple and analyzer failures, pipe plugging, and other unforeseen disturbances that may not affect the quality of the next two or three runs (and therefore will not be detected early by monitoring product quality only) but may have catastrophic effects if action is not taken.

In Part 1 of this work [4] the principles of the multivariate statistical analysis were presented. It was shown that, due to the multivariate nature of process data, univariate control charts may be deceiving. When two or more properties describe the quality of a product, the specifications should be set such that they reflect this multivariate nature of quality (two properties plotted against each other should fall within an ellipse; three properties within an ellipsoid). Two methods were presented (Principal Component Analysis and Partial Least Squares) that can be utilized to summarize large data bases by preserving their multivariate nature. The methods can project process data on lower dimensional spaces for easy inspection. Part 1 also examined ways that measurements on quality properties obtained from analytical technology during production can be combined with process data (tem-

peratures, flowrates, pH, RPM, etc) in order to provide a robust and powerful tool for real time monitoring of process and product performance. With this methodology measurements on all process variables at a given instant can be represented by one point on an index of wellness chart.

Part 2 [5] discussed the use of these methodologies to meet the needs of the Pharmaceutical Industry for batch process analysis, process understanding, monitoring, and control.

Part 3 presents more complicated approaches and addresses practical considerations for successful applications. Some of the issues discussed here are:

- ◆ Multi - Unit Process Monitoring
- ◆ Multivariate Image Technology
- ◆ Batch Process Control
- ◆ Product Transfer and Scale Up
- ◆ Integration of Clinical Data Information
- ◆ Problems with Data Acquisition and Archiving
- ◆ Practical Considerations

### Design Space, Index of Wellness, Process Signature

In Part 2 of this series [5] it was demonstrated that it is not sufficient to characterize a product with “end point quality measurements.” The reason is that the same “measured” quality properties may sometimes be achieved by taking different process paths. However, for some products we do not measure all the possible quality properties (example, downstream processability). To achieve consistency in all the product properties (measured quality and ability to process down the stream) the process conditions (path to end point) must also be kept in statistical control. When this is not the case, although the measured product properties are on target, the properties that determine other characteristics (i.e., the processability of the product) may not be within acceptable limits. Such results are corroborated from the Pharmaceutical Industry [6]. This “process path to the end point” is also discussed in the European Regulatory Perspective [7] where it is